Electron-Nuclear-Double-Resonance and Electron-Paramagnetic-Resonance Analysis of the Ytterbium-Fluorine Superhyperfine Interaction in $CaF_2:Yb^{3+}$†

U. RANON* AND JAMES S. HYDE
Varian Associates, Analytical Instrument Division, Palo Alto, California
(Received 30 August 1965)

Superhyperfine structure in the EPR spectrum of Yb^{3+} in cubic sites of CaF_2 has been investigated with EPR at both 9 Gc/sec and 35 Gc/sec and with ENDOR at 9 Gc/sec. The EPR measurements showed that the superhyperfine splitting is anisotropic and that the number of observable lines (17 at 9 Gc/sec along ⟨100⟩) and the splitting of the lines is field-dependent. ENDOR measurements permitted complete interpretation of the EPR results. The superhyperfine structure arises from coupling to the nearest-neighbor fluorine nuclei. The Hamiltonian $\mathbf{S}\cdot\mathbf{T}\cdot\mathbf{I}^F$ is used to describe the Yb^{3+}-F^- interaction where $\mathbf{T}$ has axial symmetry. The principal values are $|T_\parallel|=36.8\pm0.2$ Mc/sec and $|T_\perp|=15.9\pm0.1$ Mc/sec where $T_\parallel$ and $T_\perp$ have opposite signs. The fluorine nuclear Zeeman term and the superhyperfine interaction are of the same order, resulting in a breakdown of the usual selection rules. The number, intensity, and splitting of the EPR superhyperfine lines have been calculated with these interaction parameters and they agree well with experiment. Small shifts in the fluorine ENDOR for ^{171}Yb ($I=\frac{1}{2}$) and ^{173}Yb ($I=\frac{5}{2}$) relative to the ENDOR for the even isotopes were observed which are due to the strong hyperfine coupling in the odd isotopes. Interpretation of $T_\parallel$ and $T_\perp$ in terms of an isotropic and an anisotropic interaction is given, and results are compared with those of other workers.

I. INTRODUCTION

THE interaction between a paramagnetic impurity and the magnetic moments of ligand nuclei is observed in electron-paramagnetic-resonance spectroscopy (EPR) as an inhomogeneous broadening of the EPR lines. In some circumstances the interaction may be sufficiently strong to cause structure on each EPR line, which is referred to as superhyperfine structure (shfs).

In the rare earths the unpaired electrons are in the $4f$ shell and are shielded from the ligands by the external $5s$ and $5p$ shells. As Freeman and Watson have shown,[1] in addition to coupling from the $4f$ electrons, polarization of the $5s$ and $5p$ shells may contribute substantially to the interaction with ligand ions. However, all these interactions are usually weaker than the similar interaction of the unpaired $3d$ electrons in the iron group ions. This is because the $3d$ orbitals in these ions are in the outermost shell and are thus fully exposed to the ligands. It is not surprising therefore that superhyperfine structure in iron group EPR spectra has been observed in many cases,[2] whereas few examples have been reported for the rare earths.

Superhyperfine structure in the rare earths has been observed in Ce^{3+} in CaF_2 by Baker, Hayes, and O'Brien.[3] These authors interpreted the structure as arising from simultaneous flips of an electronic spin and fluorine nuclear spins. Low and Ranon[4] observed superhyperfine structure in the EPR spectrum of trivalent ytterbium in some thermally treated and irradiated CaF_2 crystals. This spectrum forms the basis for the present work. Extensive molecular-orbital and ligand-field calculations have been carried out on iron group elements in order to account for the observed shfs interactions,[5] but similar calculations on the rare earths have not been done.

Superhyperfine structure of other types of crystal defects not involving transition elements has also been observed in several cases. The thorough investigation of the superhyperfine structure in the spectrum of atomic hydrogen in CaF_2 by Hall and Schumacher[6] is a particularly attractive example.

The advent of electron-nuclear double resonance (ENDOR)[7] created a powerful tool for the investigation of superhyperfine interactions. By this method these interactions can be measured directly, even in the cases where they merely cause an inhomogeneous broadening of the EPR lines. In the ENDOR investigation of the superhyperfine interaction, an electronic EPR transition is partly saturated and *nuclear* reso-

† A preliminary account of this work was presented at the American Physical Society March 1965 meeting in Kansas City [Bull. Am. Phys. Soc. **10**, 329 (1965)].

* Varian Associates Postdoctoral Fellow, on leave from the Israel Atomic Energy Commission, Soreq Research Establishment, Yavne, Israel.

[1] R. E. Watson and A. J. Freeman, Phys. Rev. Letters **6**, 277 (1961).

[2] See, for example: M. Tinkham, Proc. Roy. Soc. (London) **A236**, 535 (1956); A. M. Clogston, J. P. Gordon, V. Jaccarino, M. Peter, and L. R. Walker, Phys. Rev. **117**, 1222 (1960); J. Lambe and C. Kikuchi, *ibid.* **119**, 1256 (1960); T. P. P. Hall, W. Hayes, and F. I. B. Williams, Proc. Phys. Soc. (London) **A78**, 883 (1961); P. H. Kasai, Phys. Letters **7**, 5 (1963); T. P. P. Hall, W. Hayes, R. W. H. Stevenson, and J. Wilkens, J. Chem. Phys. **38**, 1977 (1963); **39**, 35 (1963); W. Hayes and J. Wilkens, Proc. Roy. Soc. (London) **A281**, 340 (1964); D. Van Ormondt and T. Thalhammer, Phys. Letters **14**, 169 (1965); C. Kikuchi, I. Chen, W. H. From, and P. B. Dorain, J. Chem. Phys. **42**, 181 (1965); I. Chen, C. Kikuchi, and H. Watanabe, J. Chem. Phys. **42**, 189 (1965); J. H. M. Thornley, C. G. Windsor, and J. Owen, Proc. Roy. Soc. (London) **A284**, 252 (1965) and references therein.

[3] J. M. Baker, W. Hayes, and M. C. M. O'Brien, Proc. Roy. Soc. (London) **A254**, 273 (1960).

[4] W. Low and U. Ranon, *1st International Conference on Paramagnetic Resonance, Jerusalem, 1962*, edited by W. Low (Academic Press Inc., New York, 1963), p. 167.

[5] Most papers listed in Ref. 2 deal with these problems. See also: J. Owen, Discussions Faraday Soc. **19**, 127 (1955); A. Mukherji and T. P. Das, Phys. Rev. **111**, 1479 (1958); F. Keffer, T. Oguchi, W. O'Sullivan, and J. Yamashita, *ibid.* **115**, 1553 (1959); W. Marshal and R. Stuart, *ibid.* **123**, 2048 (1961); K. Knox, R. G. Shulman, and S. Sugano, *ibid.* **130**, 506, 512, 517 (1963); R. G. Shulman and S. Sugano, J. Chem. Phys. **42**, 39 (1965); I. Chen, C. Kikuchi, and H. Watanabe, *ibid.* **42**, 186 (1965).

[6] J. L. Hall and R. T. Schumacher, Phys. Rev. **127**, 1892 (1962); see also: B. Welber, *ibid.* **136**, A1408 (1964).

[7] G. Feher, Phys. Rev. **103**, 500, 843 (1956); **114**, 1219 (1959).

nance transitions are induced simultaneously in the ligand nuclei. The resonance frequency of the ligand nuclei is measured by plotting the change in the EPR signal while sweeping the nuclear rf. For optimum ENDOR sensitivity, the nuclei have to be flipped at a rate which is comparable with the electronic relaxation time. The intensity of the magnetic component, H_{rf}, of the nuclear rf field at the sample should be of the order of $1/\gamma T_1$ where T_1 is the electronic spin-lattice relaxation time and γ is the nuclear gyromagnetic ratio. For $T_1=10^{-3}$ sec, $H_{rf}\sim\frac{1}{4}$ G, which can be achieved easily. With decreasing relaxation times and accordingly increasing rf power requirements however, the experiment becomes more difficult.

The relaxation times of most of the rare-earth ions are much shorter than those of the iron-group ions. Presumably this is due mainly to the fact that in the rare earths the orbital angular momentum of the electrons is not quenched by the crystal field, whereas in the iron group (as well as in other *nd* groups) the strong crystal-field interaction results in an almost total quenching of the orbital momentum. Therefore the observation of ENDOR with rare-earth ions at a given temperature requires higher nuclear rf power than for most iron group ions. The exceptions are divalent europium and trivalent gadolinium which are *S*-state ions and thus have relatively long relaxation times.

ENDOR experiments on rare-earth ions and on the fluorine ligands in CaF_2 have been performed on Eu^{2+} by Baker *et al.*[8,9] and on Tm^{2+} by Bessent and Hayes.[10]

The spin lattice relaxation times of most of the trivalent rare-earth ions in calcium fluoride have been measured by Bierig *et al.*[11] For Yb^{3+} in cubic sites they find $T_1\approx 20\,\mu$sec at 15°K and $T_1\approx 150\,\mu$sec at 4°K. At 15°K $1/\gamma T_1$ is of the order of 12.5 G, and in order to get good ENDOR signals one has to introduce a nuclear rf power with H_{rf} of the order of tens of gauss into the sample cavity. Very little is known about ENDOR signal intensities as a function of temperature. A necessary condition for ENDOR is that $T_1<T_x$ where T_x is the cross relaxation time. This suggests that superior overall ENDOR signal intensities can be achieved in some cases by operating at relatively high temperature and high rf power.

An ENDOR spectrometer which can achieve an H_{rf} of 40 G in the rotating frame has been constructed in this laboratory and applied successfully to the study of ENDOR in liquids[12,13] and in organic crystals.[14] This spectrometer has been modified so that it could be operated in the desired temperature range for the Yb^{3+} investigation. Both ENDOR experiments and *X*-band EPR experiments at 15°K were carried out on this instrument.

The structure of CaF_2 is cubic, and can be visualized as a simple cubic array of F^- ions with a divalent calcium ion at the body centers of alternate cubes. The rare-earth ions substitute for Ca^{2+} but usually go into the crystal as trivalent ions. Compensation for the excess positive charge occurs in several ways and gives rise to different local symmetries of the crystalline field at the rare-earth-ion sites.[15] In this paper we shall be concerned only with the EPR spectrum of Yb^{3+} in cubic sites in single crystals of CaF_2, although other site symmetries have been observed in the CaF_2:Yb^{3+} system.

The EPR spectrum of trivalent ytterbium in calcium fluoride was first measured by Low.[16] The g value given in Low's paper is incorrect because of a typographical error.[16a] It was remeasured by Hayes and Twidell[17] and by Ranon.[18]

The configuration of Yb^{3+} is $4f^{13}$ and the lowest state of the free ion by Hund's rule is $^2F_{7/2}$. In a cubic field the $J=\frac{7}{2}$ multiplet is split into two doublets, Γ_6 and Γ_7, and a quartet Γ_8. The point-charge model of the crystal field predicts that in an eightfold cubic coordination, as is the case here, Γ_7 should be the lowest state, with a g value of 3Λ where $\Lambda=8/7$ is the Landé factor.

The EPR spectrum consists of an intense central line at $g=3.443\pm0.002$, which is very close to 3Λ—showing that the ground state is indeed Γ_7. This line is due to a number of even ytterbium isotopes which comprise a total of about 70% of the natural abundance of ytterbium. The rest of the spectrum consists of (a) a two-line hyperfine pattern due to ^{171}Yb($I=\frac{1}{2}$), and (b) a six-line hyperfine pattern due to ^{173}Yb($I=\frac{5}{2}$). These isotopes have a natural abundance of 14 and 16%, respectively.

The main features of the EPR spectrum are described by an isotropic spin Hamiltonian of the form[16–18]

$$\mathcal{H}=g\beta\mathbf{H}\cdot\mathbf{S}+A\mathbf{S}\cdot\mathbf{I}$$

with the parameters

$$g=3.443\pm0.002$$

$$^{171}A=(2658\pm4.5)\text{ Mc/sec}\quad ^{173}A=(-729\pm1.2)\text{ Mc/sec.}$$

The present work stems from an effort to understand the superstructure in the CaF_2:Yb^{3+} spectrum.[4] This

[8] J. M. Baker and F. I. B. Williams, Proc. Roy. Soc. (London) **A267**, 283 (1962).
[9] J. M. Baker and J. P. Hurrell, Proc. Phys. Soc. (London) **82**, 742 (1963).
[10] R. G. Bessent and W. Hayes, Proc. Roy. Soc. (London) **A285**, 430 (1965).
[11] R. W. Bierig, M. J. Weber, and S. I. Warshaw, Phys. Rev. **134**, A1504 (1964); see also, Chao-Yuan Huang, *ibid.* **139**, A241 (1965).
[12] J. S. Hyde and A. H. Maki, J. Chem. Phys. **40**, 3117 (1964).
[13] J. S. Hyde, J. Chem. Phys. **43**, 1806 (1965).
[14] A. L. Kwiram and J. S. Hyde, J. Chem. Phys. **42**, 791 (1965).
[15] For a recent summary of EPR results on rare earth doded CaF_2, see: M. J. Weber and R. W. Bierig, Phys. Rev. **134**, A1492 (1964).
[16] W. Low, Phys. Rev. **118**, 1608 (1960).
[16a] W. Low (private communication).
[17] W. Hayes and J. W. Twidell, J. Chem. Phys. **35**, 1521 (1961).
[18] U. Ranon, thesis, The Hebrew University, Jerusalem 1963 (unpublished).

reported structure showed 13 closely spaced lines superimposed on the central $(I=0)Yb^{3+}$ EPR line, when observed at X band at 20°K along a ⟨100⟩ axis. When the external magnetic field is oriented along a cube axis all eight fluorine nuclei which surround a Yb^{3+} ion are equivalent. Fluorine nuclei have a spin $I^F=\frac{1}{2}$ and one would therefore expect to see

$$2\sum_{i=1}^{8} I_i^F+1=9$$

superhyperfine lines of the usual $\Delta I_z^F=0$ type, which is the selection rule prevailing in ordinary EPR hyperfine spectra. Low and Ranon[4] discussed some models, trying to account for the observed 13 lines, but no satisfactory interpretation could be given. It was found in the present work that ENDOR experiments on ligand fluorine nuclei were essential for the interpretation of this superhyperfine structure.

Instrumentation and experimental details are described in Part II. In Part III an account is given of the various EPR experiments which were carried out in an effort to explain the superhyperfine structure, and the results are listed. A theoretical discussion of the problem is presented in Part IV, and the ENDOR results are given in Part V. The correlation of the ENDOR results with the EPR data is discussed in Part VI. Shifts of the fluorine ENDOR frequency for ^{171}Yb and ^{173}Yb which are caused by the strong hyperfine coupling of the electrons to the Yb nuclear moments are also discussed in Part VI.

II. INSTRUMENTATION

1. ENDOR Apparatus

A detailed description of the ENDOR spectrometer has been published elsewhere.[13] Since the instrumentation is somewhat unusual, it seems appropriate to describe it here in abbreviated form.

The spectrometer was constructed around a Varian V-4500 EPR spectrometer which employs a cylindrical cavity operating in a TE_{011} mode. The design of this cavity is such that the cylindrical walls are transparent to transverse rf magnetic fields and the top and bottom of the cavity are electrically insulated from each other. The rf coil consists of a one-turn loop formed by the metallic end walls of the cavity and straps down the sides of the cavity. See Fig. 1.

The microwave cavity and radio-frequency coil are at ambient temperature (nominally 100°C when the rf power is on). Samples were glued to a rexolite rod which in turn was glued to a quartz rod inserted into a transmission Dewar (Varian V-4546) extending through the cavity. The cooling of the sample in the range 9–20°K was achieved by passing helium gas from a liquid-helium storage Dewar to the glass Dewar by means of a specially constructed transfer tube. Helium was evaporated in the storage Dewar by passing current through

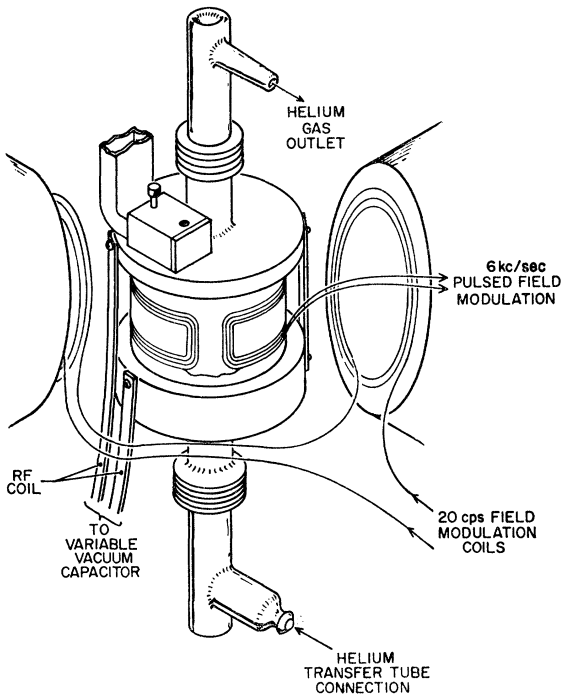

FIG. 1. The cavity structure showing the rf coupling and sample cooling arrangement.

a 200-Ω wire-wound resistor. A temperature of 15°K at the sample could be achieved with a power input of 1 W evaporating about 1 liter of liquid He per hour. At 5 liters per hour a sample temperature of 9°K could be achieved.

The design objective of the ENDOR spectrometer was to achieve intense nuclear radio-frequency fields. A transmitter providing one kilowatt rf power in the frequency range of 10–30 Mc/sec was constructed. To increase the intensity of the rf magnetic field of the sample, the rf coil was made part of a parallel resonant circuit ($Q\sim15$). In this way fields of 40 G in the rotating frame can be achieved.

The radio-frequency power is pulsed with a limited duty cycle, in order to reduce heating of the microwave cavity. The input to the receiver is gated by the same pulser which gates the rf power. Hence all noise generated when the rf is off is eliminated from the integrating circuit which follows the final detector.

In order to eliminate spurious signals caused by the intense nuclear rf power, the signal is coded to a high degree and decoded in a strongly discriminating circuit. See the block diagram, Fig. 2. The frequency of the rf oscillator is square-wave modulated at 6 kc/sec, and the rf power amplifier is gated at 12 kc/sec (pulse duration 10 μsec). Alternate rf pulses are then at different frequencies. The difference of the alternate pulses may be adjusted to a value somewhat less than the ENDOR linewidth (50 to 300 kc/sec), and the average radio frequency can be swept. The signal from

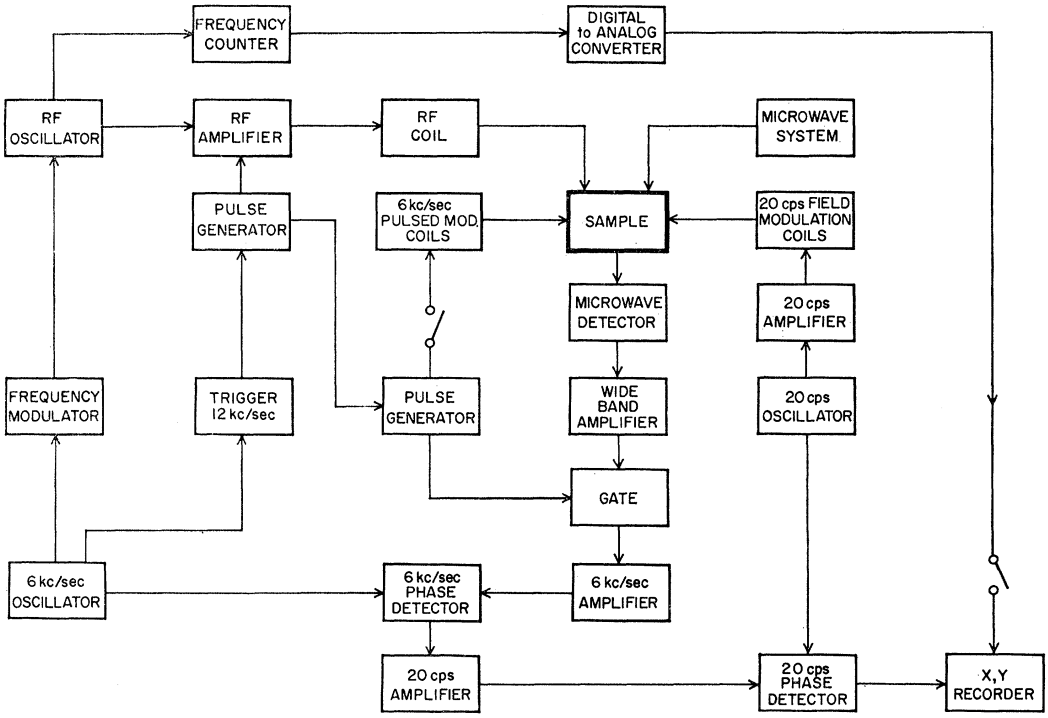

FIG. 2. Block diagram of the ENDOR spectrometer.

the microwave detector is amplified and passed through a gated switch into a narrow-band amplifier tuned to 6 kc/sec. This amplifier passes only the first Fourier component of the signal pulse. The Fourier component at 6 kc/sec has an intensity proportional to the difference in signals detected at the alternate frequencies,[13] and an ENDOR display resembling the derivative of a pure absorption is obtained. Additional baseline stability was achieved by employing field modulation at 20 cps. The output of the 6-kc/sec phase-sensitive detector is amplified and phase-sensitive-detected at 20 cps.

A particularly convenient ENDOR data display is also shown in the block diagram Fig. 2. The radio frequency from the oscillator is measured by an HP 5245L electronic counter (a mean frequency is measured in the case of alternate pulses). The counter is coupled to an HP 380A digital-to-analog converter which converts the frequency to an analog dc voltage. This voltage is fed to the X axis of an X-Y recorder, the Y axis of which is driven by the signal.

2. EPR Apparatus

X band. For observation of ordinary EPR, using the ENDOR spectrometer, pulses of current are driven through additional field modulation coils mounted on the cavity structure (see Fig. 1). A repetition rate of 6 kc/sec is used. Thus as far as ordinary EPR is concerned, the instrument is a double modulation spectrometer. The double phase detection at 6 kc/sec and 20 cps results in a recorded signal which is the second derivative of the absorption line.

35 Gc/sec. The EPR experiments at 35 Gc/sec and 4°K were carried out on a Varian V-4503 EPR spectrometer. The field modulation frequency was 400 cps, and a 9-in. rotating magnet was employed.

III. EPR EXPERIMENTS

The experiments reported here were performed on CaF_2:Yb^{3+} crystals obtained from Optovac Inc. The crystals were transparent and had a nominal concentration of 0.1 $M\%$ Yb^{3+}. They were glued to rexolite mounts designed to permit rotation in either the (100) or the (110) planes.

The EPR spectrum at X band with the external field oriented along a ⟨100⟩ axis is shown in Fig. 3. In addition to the main cubic spectrum, two lines of Yb^{3+} in tetragonal sites are seen[15,19] in the figure at 1900 and 1685 G. We shall not be concerned with this anisotropic spectrum in the present work.

A striking feature of this figure is the clearly observed superhyperfine structure on all cubic EPR lines. It is interesting to note also the apparent increase in the superstructure line intensity of each Yb^{3+} isotope as the magnetic field increases. This intensity variation is discussed in Part VI.

The central line, when observed under much higher resolution, is shown in Fig. 4. There are 17 components

[19] U. Ranon and A. Yaniv, Phys. Letters **9**, 17 (1964).

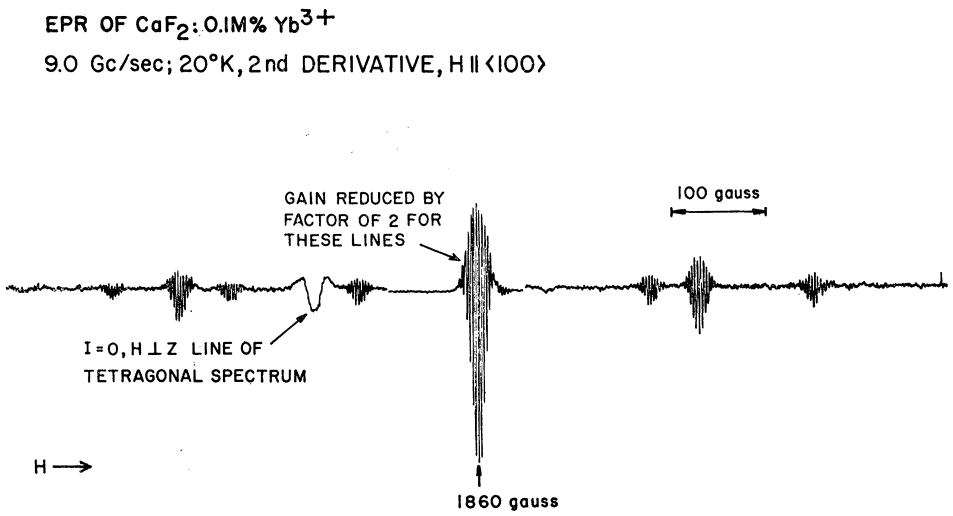

FIG. 3. The EPR spectrum of Yb^{3+} in cubic sites in CaF_2 at X band with the external field along a cube axis, showing the hyperfine and superhyperfine structures.

in this superhyperfine structure with the relative intensities listed in the second row of Table I. The separation between the superhyperfine structure lines in this case is 3.03±0.05 G.

TABLE I. Measured and calculated relative intensities of the superhyperfine EPR lines for the even isotopes of Yb^{3+}; **H** along ⟨100⟩ at X band.

Shfs line	0	±1	±2	±3	±4	±5	±6	±7	±8
Measured	275	255	208	146	85	37	13	2±1	···
Calculated	275	253	203	136	78	36	13.6	3.4	0.7

A comparison of the shfs on the two ^{171}Yb lines is shown in Fig. 5. It is seen that the splittings are different, indicating that the shfs is field-dependent. The splittings are 2.97±0.07 G and 3.2±0.05 G for the low- and high-field lines, respectively. The magnetic-field-dependent variation in splitting is very small over the EPR linewidth. In the discussions which follow, the separation between the shfs lines on each ytterbium EPR hyperfine line is assumed to be constant.

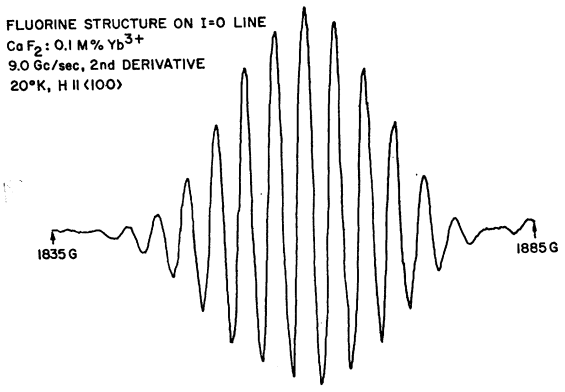

FIG. 4. The superhyperfine structure on the central EPR line (even isotopes) of Yb^{3+} at X band with the external field along a cube axis.

When the magnetic field is rotated away from the ⟨100⟩ direction the superstructure disappears. At X band a new superstructure is observed with the field parallel to a ⟨110⟩ direction. This is shown in Fig. 6. Only 13 lines are observed, with relative intensities close to those for the ⟨100⟩ orientation. The separation between the lines is 3.55±0.1 G. The superstructure lines are somewhat broader in this case than in the ⟨100⟩ orientation.

A strong dependence of the shfs resolution on temperature was found. Figure 7 shows the central Yb^{3+} line with the magnetic field along ⟨100⟩ at 15°K and 4°K. The marked change in resolution cannot be ascribed to temperature variation of the superhyperfine interaction since the ENDOR measurements show that this interaction is temperature-independent between 9–15°K. The resolution did not change when the microwave power was varied. This puzzling behavior is not understood. Baker *et al.*[3] reported a strong tem-

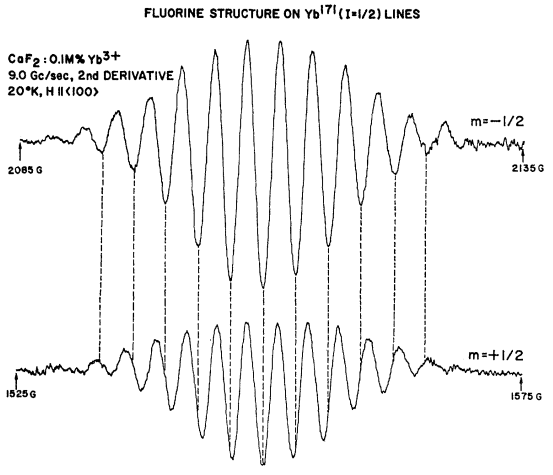

FIG. 5. The superhyperfine structure on the EPR lines of $^{171}Yb^{3+}$ ($I=\frac{1}{2}$) at X band along the cube axis, showing the field dependence of the superhyperfine splitting.

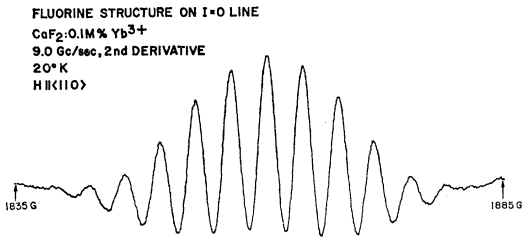

FIG. 6. Superhyperfine structure on the central EPR line (even isotopes) of Yb^{3+} at X band with the external field along a $\langle 110\rangle$ orientation.

perature dependence of the shfs in Ce^{3+}-doped CaF_2 which was explained as the result of the temperature dependence of the spin lattice relaxation time. This explanation does not appear sufficient in the present case.

Although the EPR spectrum at 4°K and X band revealed very little superhyperfine structure, measurements at 4°K and 35 Gc/sec showed a fairly well resolved shfs along $\langle 100\rangle$ only. This is shown in Figs. 8 and 9. The separation between the superhyperfine lines along $\langle 100\rangle$ is 6.65 ± 0.1 G.

The various EPR experiments indicated that fluorine nuclear flips must be involved in the observed shfs. However, the large number of shfs lines at X band and their strong intensities remained somewhat of a puzzle until the ENDOR experiments were carried out. In the case of Ce^{3+} in CaF_2, the lines associated with the fluorine flips were an order of magnitude weaker[3] than the so-called allowed transitions which did not involve a nuclear flip.

The numerical EPR results are summarized in Tables I and IV.

IV. THEORY

1. The EPR Spectrum

The ytterbium-fluorine system can be described by a spin Hamiltonian of the form

$$\mathcal{H}=\beta\mathbf{H}\cdot\mathbf{g}\cdot\mathbf{S}+\mathbf{S}\cdot\mathbf{A}\cdot\mathbf{I}+P[I_z^2-\tfrac{1}{3}I(I+1)]+\sum_i(\mathbf{S}\cdot\mathbf{T}_i\cdot\mathbf{I}_i^F-\gamma_N{}^F\mathbf{H}\cdot\mathbf{I}_i^F), \quad (1)$$

with an effective spin $S=\frac{1}{2}$. The first three terms in (1) are the electronic Zeeman term, the ^{171}Yb or ^{173}Yb hyperfine terms, and the quadrupole interaction of ^{173}Yb. The first summation term represents the superhyperfine interaction between the Yb^{3+} ion and the fluorine nuclei with nuclear spin $I_i^F=\frac{1}{2}$. The superhyperfine interaction tensor is given by $\mathbf{T}_i$, and the sum is taken over all the interacting nuclei. The second summation is the fluorine nuclear Zeeman term taken over the interacting nuclei.

A fluorine-fluorine nuclear dipole interaction term of the form $\sum_{i,j}\mathbf{I}_i^F\cdot\mathbf{B}_{ij}\cdot\mathbf{I}_j^F$ has been neglected since it is expected to be very small. The F^--F^- separation in CaF_2 is 2.73 Å, yielding a classical dipole-dipole interaction of 2.5 kc/sec which is $\sim$0.5 mG in the EPR spectrum. Similarly, the Yb nuclear Zeeman term has been neglected. This interaction, of the form $\gamma_N\mathbf{H}\cdot\mathbf{I}$, shifts the hyperfine levels of both odd ytterbium isotopes by less than 0.5 G, but does not affect either the hyperfine or superhyperfine structure.

In a cubic field the g tensor for Yb^{3+} is isotropic since the ground state is a Kramers doublet, the ytterbium hyperfine interaction tensor $\mathbf{A}$ is isotropic, and the gradient of the electric field at the center of symmetry vanishes so that $P=0$. Choosing the external field as the z axis, the spin Hamiltonian will be

$$\mathcal{H}=g\beta HS_z+A\mathbf{I}\cdot\mathbf{S}+\sum_i(\mathbf{S}\cdot\mathbf{T}_i\cdot\mathbf{I}_i^F-\gamma_N{}^F\mathbf{H}\cdot\mathbf{I}_i^F). \quad (2)$$

The fluorine nuclear Zeeman term gives a splitting of about 1.5 G at X band and our experiments show that the superhyperfine splittings are of the order of $\sim$3 G. Thus, the two last terms in (2) are of the same order of magnitude and neither can be neglected in further diagonalization of (2). Both terms are much smaller than A and can be treated as perturbations on the hyperfine eigenstates of the Yb^{3+} ions. The hyperfine eigenvalues to second order are

$$E(S_z,I_z)=g\beta HS_z+AS_zI_z+(A^2/2h\nu)[I(I+1)-I_z(I_z+2S_z)], \quad (3)$$

where $S_z=\pm\frac{1}{2}$, $^{171}I_z=\pm\frac{1}{2}$ and $^{173}I_z=\pm\frac{5}{2}, \pm\frac{3}{2}, \pm\frac{1}{2}$.

In the exact calculation of the ^{171}Yb EPR spectrum, higher order terms must be included because ^{171}A is very large; however, we shall be interested only in the influence of this hyperfine coupling on the ENDOR spectrum and for this purpose expression (3) will be adequate.

The superhyperfine tensor $\mathbf{T}_i$ must be expressed in explicit form before the superhyperfine perturbation can be calculated. The discussion is confined to the first shell of fluorines surrounding the Yb^{3+} ions since it will be shown that this shell gives rise to the observed superhyperfine structure.

Substitution of trivalent ytterbium at sites of divalent calcium ions causes an axial distortion of the

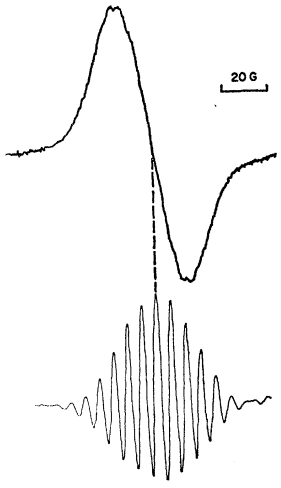

FIG. 7. Dependence of the superhyperfine resolution on temperature. Lower Trace: Central EPR line at X band along $\langle 100\rangle$ at 15°K (second derivative). Upper Trace: Same line at 4°K (first derivative).

crystal field at the nearest neighbor fluorine sites when the Yb sites possess local cubic symmetry. The F^--Yb^{3+} axis of distortion coincides with a cube body diagonal, which is labeled the z' axis. The superhyperfine tensor will be diagonal in a coordinate system where z is parallel to z' and will have axial symmetry in this system. The components of $\mathbf{T}$ will be $T_{\parallel}$ along z' and $T_{\perp}$ in a plane perpendicular to z'. In the primed coordinate system the superhyperfine term will have the form

$$T_{\parallel}S_{z'}I_{z'}+T_{\perp}(S_{x'}I_{x'}+S_{y'}I_{y'}). \tag{4}$$

We want to express $\mathbf{T}_i$ in the unprimed coordinate system. Taking the origin on the Yb^{3+} ion and denoting by θ_i the angle subtended at the origin by the external field and the body diagonal to the ith fluorine, $\mathbf{T}_i$ has the form

$$\mathbf{T}_i=\begin{bmatrix} T_{\parallel}\sin^2\theta_i+T_{\perp}\cos^2\theta_i & 0 & (T_{\parallel}-T_{\perp})\sin\theta_i\cos\theta_i \\ 0 & T_{\perp} & 0 \\ (T_{\parallel}-T_{\perp})\sin\theta_i\cos\theta_i & 0 & T_{\parallel}\cos^2\theta_i+T_{\perp}\sin^2\theta_i \end{bmatrix}, \tag{5}$$

where z is now parallel to $\mathbf{H}$.

Most of our experiments were carried out on the central line of the Yb^{3+} EPR spectrum and, therefore, we take $A=0$ in (2). The case with $A\neq 0$ will be treated in Part VI.

The Hamiltonian becomes

$$\mathcal{H}=g\beta HS_z+\sum_{i=1}^{8}(\mathbf{S}\cdot\mathbf{T}_i\cdot\mathbf{I}_i^F-\gamma_N{}^F\mathbf{H}\cdot\mathbf{I}_i^F), \tag{6}$$

where $\mathbf{T}_i$ is given by (5) and the sum is taken over the eight nearest neighbor fluorines. Fluorine ions situated at opposite cube corners along a particular body diagonal are equivalent since they are related to each other by inversion through the origin. Therefore, for any orientation of the external field there will be at most four different $\mathbf{T}_i$ tensors in (6).

For the even ytterbium isotopes the spin $\mathbf{S}$ is oriented along the external field direction and $\mathbf{S}\approx S_z$ in

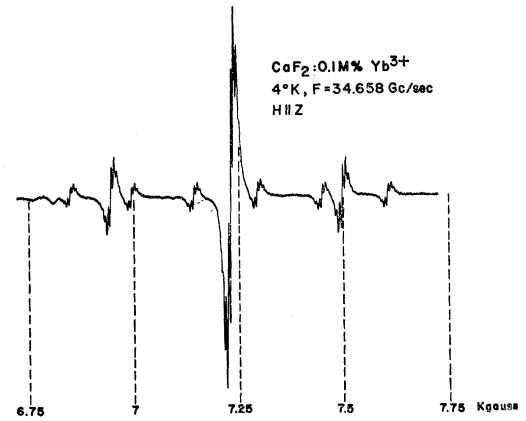

FIG. 8. The EPR spectrum of Yb^{3+} in cubic sites in CaF_2 at 35 Gc/sec, 4°K with the external field along a cube axis.

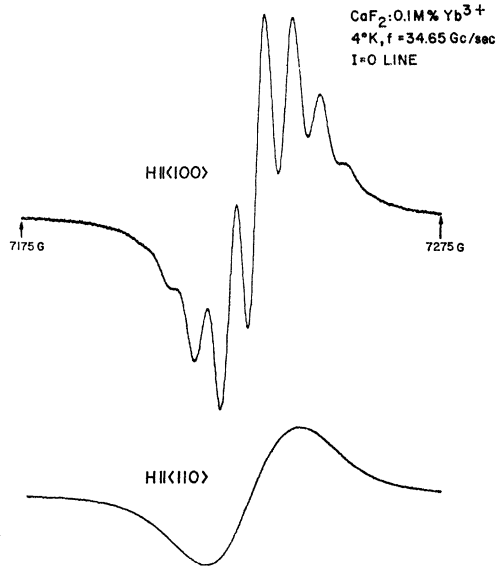

FIG. 9. The central line of the Yb^{3+} EPR spectrum at 35 Gc/sec, 4°K with the field along ⟨100⟩ and ⟨110⟩.

(6). This amounts to neglect of off-diagonal elements of $\mathbf{S}$ in (6). The elements of $\mathbf{T}_i$ are of the order of 3 G. The off-diagonal elements of $\mathbf{S}$ introduce shifts in the energy levels of the order of ζ^2/H_0, where $\zeta\approx 3$ G. At X band, $H_0\approx 1900$ G and $\zeta^2/H_0\approx 5$ mG. This is much less than the observed linewidth of the superhyperfine lines, as can be seen in Figs. 4–7. It amounts to only a few tens of cycles in the fluorine nuclear resonance frequency. Thus the neglect of the off-diagonal terms of $\mathbf{S}$ in (6) is justified.

Each component in the sum in (6) can be treated separately since there are no matrix elements connecting the different fluorine nuclear spins. Accordingly we want to diagonalize the Hamiltonian

$$\mathcal{H}_F=\mathbf{S}\cdot\mathbf{T}\cdot\mathbf{I}^F-\gamma_N{}^FHI_z{}^F, \tag{7}$$

where $S=S_z$ and the subscript i has been omitted. Using (5) we have

$$\mathcal{H}=S_z(T_{\parallel}-T_{\perp})\sin\theta\cos\theta I_x{}^F +[S_z(T_{\parallel}\cos^2\theta+T_{\perp}\sin^2\theta)-\gamma_N{}^FH]I_z{}^F. \tag{8}$$

The diagonalization of this Hamiltonian in the $(S_z, I^F=\frac{1}{2})$ manifold is straightforward and yields the eigenvalues

$$E^F(S_z,I_z)=I_z{}^F[(S_zT_{\parallel}-\gamma_N{}^FH)^2\cos^2\theta +(S_zT_{\perp}-\gamma_N{}^FH)^2\sin^2\theta]^{1/2}. \tag{9}$$

This expression may be rewritten

$$E^F(S_z,I_z{}^F)=I_z{}^F(P^2\cos^2\theta+Q^2\sin^2\theta)^{1/2}, \tag{10}$$

where

$$\begin{aligned} P&=S_zT_{\parallel}-\gamma_N{}^FH, \\ Q&=S_zT_{\perp}-\gamma_N{}^FH. \end{aligned} \tag{11}$$

The energy levels of the even Yb^{3+} isotopes may be calculated from the expression

$$E=g\beta HS_z+\sum_{i=1}^{8} I^F{}_{z,i}[P^2\cos^2\theta_i+Q^2\sin^2\theta_i]^{1/2} \quad (12)$$

by letting $S_z=\pm\frac{1}{2}$, $I^F{}_{z,i}=\pm\frac{1}{2}$ and remembering that P and Q depend on S_z.

2. Electronic Transition Probabilities

In this section a simple method is developed for calculation of the intensities of the superhyperfine lines. The intensities of the lines from an ytterbium-fluorine pair are determined first, and then the total spectrum is found by superimposing on the pure Yb^{3+} electronic transitions the interactions with the eight fluorine nuclei taking these one at a time.

For a ytterbium-fluorine pair, four electronic levels exist. These are superhyperfine levels arising from the splitting into two of each of the two ytterbium Zeeman levels by the fluorine nuclear spin. In principle, therefore, four electronic transitions are possible. The transition probabilities will depend on the eigenfunctions describing the states.

In the ordinary EPR hyperfine spectra where the hyperfine structure arises from the electronic-nuclear interaction in the paramagnetic ion, the eigenfunctions of the states are determined by the condition.

$$\text{(Electron Zeeman energy)}\gg\text{(hyperfine energy)}\gg\text{(nuclear Zeeman energy)}. \quad (13)$$

The 4 electronic states are adequately described by functions of the form $|S_z\rangle|I_z\rangle$. Therefore, two of the four possible EPR transitions, namely those which involve $\Delta I_z=\pm 1$, have zero intensity.

There are cases, however, where the hyperfine interaction and the nuclear Zeeman terms are of the same order of magnitude. Such a situation occurs frequently in organic free radicals. In the case of CaF_2:Yb^{3+} the EPR spectrum shows that the elements of $\mathbf{T}$ are of the order of 10 Mc/sec. The nuclear magnetic moment of fluorine is 2.627 nuclear magnetons and at X band the nuclear Zeeman term amounts to about 7.5 Mc/sec. Thus, using a semiclassical picture, the magnetic field due to the magnetic electrons of the paramagnetic ion acting on the fluorine nuclei is of the same order as the external field. Consequently, the fluorine nuclear axis of quantization will be along the resultant of the external and electronic fields and the two resultants for the two *electronic* states will not be antiparallel.

Call the unit vectors along the direction of the resultant field for the two electronic states ζ and η, respectively. Let ϕ be the angle between the two resultant fields. Take the initial states along ζ to be $|+\rangle$ and $|-\rangle$. It can be shown that the final nuclear states, along η, are[20]

$$\begin{aligned}|+\rangle^\dagger&=\cos(\phi/2)|+\rangle+\sin(\phi/2)|-\rangle,\\ |-\rangle^\dagger&=-\sin(\phi/2)|+\rangle+\cos(\phi/2)|-\rangle.\end{aligned} \quad (14)$$

The transition probabilities are then:

$$\text{for } |+\rangle\rightarrow|+\rangle^\dagger \text{ and } |-\rangle\rightarrow|-\rangle^\dagger,\quad \cos^2(\phi/2); \quad (15)$$

$$\text{for } |+\rangle\rightarrow|-\rangle^\dagger \text{ and } |-\rangle\rightarrow|+\rangle^\dagger,\quad \sin^2(\phi/2). \quad (16)$$

In ordinary electron-nuclear hyperfine interactions where (13) prevails, $\phi\approx\pi$ and $\cos\frac{1}{2}\phi\approx 0$ so that only two transitions will have appreciable intensities. On the other hand, in cases where the electron-nuclear interaction is of the same magnitude as the nuclear Zeeman energy, one would expect to see two pairs of EPR lines whose relative intensities depend entirely on the angle ϕ. This angle in turn is dependent on the relative magnitude of the electron-nuclear and nuclear Zeeman interactions. Cases exist where the "forbidden" transitions (15) are more intense than the allowed ones (16). The problem of these relative intensities has been treated in detail by McConnell *et al.*[21] These authors have investigated some organic free radicals and given detailed description of the expected intensities of the hyperfine lines under various conditions.

In order to calculate ϕ explicitly it is convenient to follow Hall and Schumacher[6] and write the Hamiltonian (7) in the form

$$\mathcal{H}_F=\gamma_N{}^F[(1/\gamma_N{}^F)(\mathbf{S}\cdot\mathbf{T})-\mathbf{H}]\cdot\mathbf{I}^F=\gamma_N{}^F\mathbf{H}_t\cdot\mathbf{I}^F, \quad (17)$$

where $\mathbf{H}_t=(1/\gamma_N{}^F)(\mathbf{S}\cdot\mathbf{T})-\mathbf{H}$ is the total (resultant) magnetic field acting on a fluorine nucleus. Since we have $\mathbf{S}\approx S_z$ and $\mathbf{H}=H_z$, $\mathbf{H}_t$ will have the components

$$\mathbf{H}_t(S_z)=\frac{1}{\gamma_N{}^F}[S_z(T_{\parallel}-T_\perp)\sin\theta\cos\theta,\ 0,\ S_z(T_{\parallel}\cos^2\theta+T_\perp\sin^2\theta)-\gamma_N{}^F H] \quad (18)$$

and ϕ will be given by

$$\cos\phi=[\mathbf{H}_t(+)\cdot\mathbf{H}_t(-)]/|H_t(+)||H_t(-)|. \quad (19)$$

Here $(+)$ and $(-)$ stand for $S_z=+\frac{1}{2}$, $-\frac{1}{2}$, respectively. From (18), (19), and (11) we then get

$$\cos\phi=\frac{P_+P_-\cos^2\theta+Q_+Q_-\sin^2\theta}{[P_+{}^2\cos^2\theta+Q_+{}^2\sin^2\theta]^{1/2}[P_-{}^2\cos^2\theta+Q_-{}^2\sin^2\theta]^{1/2}}, \quad (20)$$

where the subindices $+$, $-$ stand for $S_z=+\frac{1}{2}$, $-\frac{1}{2}$ in (11).

In order to calculate the total EPR superhyperfine spectrum arising from the interaction with the eight nearest-neighbor fluorine nuclei, expression (20) has to be evaluated for each nucleus and the transition

[20] E. M. Corson, *Perturbation Methods in the Quantum Mechanics of n-Electron Systems* (Blackie & Son Ltd., London, 1951), p. 116.

[21] H. M. McConnell, C. Heller, T. Cole, and R. W. Fessenden, J. Am. Chem. Soc. **82**, 766 (1960).

probabilities calculated from (15) and (16). The 4 lines from the first Yb-F pair are spaced according to Eq. (12), each of the 4 lines is split into a quartet by introducing a second fluorine nucleus, each in turn is split again by the third nucleus, etc. and in this manner the spectrum can be constructed.

Clogston *et al.*[22] have calculated general expressions for both the positions and relative intensities of shfs lines in cases where the local field at the paramagnetic ion is rhombic. These expressions are of necessity quite complicated. The expressions derived here are special cases of the general expressions of Clogston *et al.* The merit of deriving and using the expressions given in the present paper lies in the simplicity of their derivation and application, although their usefulness is limited to the cases where the paramagnetic ions are situated at sites of cubic symmetry. A calculation of hyperfine splitting for cases where the hyperfine interaction and nuclear Zeeman terms are of the same order of magnitude has been given also by Woodbury and Ludwig.[23]

3. The ENDOR Spectrum

The transitions which are observed in an ENDOR spectrum are between adjacent superhyperfine levels in a constant S_z state. For a particular fluorine nucleus we have from (10)

$$h\nu_n=[P^2\cos^2\theta+Q^2\sin^2\theta]^{1/2} \tag{21}$$

where ν_n is the ENDOR transition frequency.

Equation (21) can be written in the form

$$\nu_n^2=P^2+(Q^2-P^2)\sin^2\theta, \tag{22}$$

where P and Q are measured in Mc/sec. By plotting ν_n versus $\sin^2\theta$ the parameters $|P|$ and $|Q|$ can be determined. $T_{\parallel}$ and $T_{\perp}$ cannot be separated from $\gamma_N{}^F H$ by performing an ENDOR experiment at a single setting of the external field since only $|P|$ and $|Q|$ are measured. In addition $T_{\parallel}$ and $T_{\perp}$ cannot be determined in such an experiment because: (a) The signs of $T_{\parallel}$ and $T_{\perp}$ are not known *a priori*, and (b) for an $S=\frac{1}{2}$ doublet there is no way to tell whether the $S_z=+\frac{1}{2}$ or $S_z=-\frac{1}{2}$ state is observed. By measuring the ENDOR at two different settings of the external field, however, values for $|S_zT_{\parallel}|$ and $|S_zT_{\perp}|$ can be derived. This has been done in the present investigation by performing ENDOR experiments on the various EPR hyperfine lines of ytterbium. A detailed discussion of these measurements is given in Part V.

V. ENDOR EXPERIMENTAL RESULTS

Most of the ENDOR experiments on the central line of the EPR spectrum were performed at about 12–15°K using the helium-gas-flow technique described previously. This temperature range was obtained with a power input of 2.5–1.5 W into the helium bath.

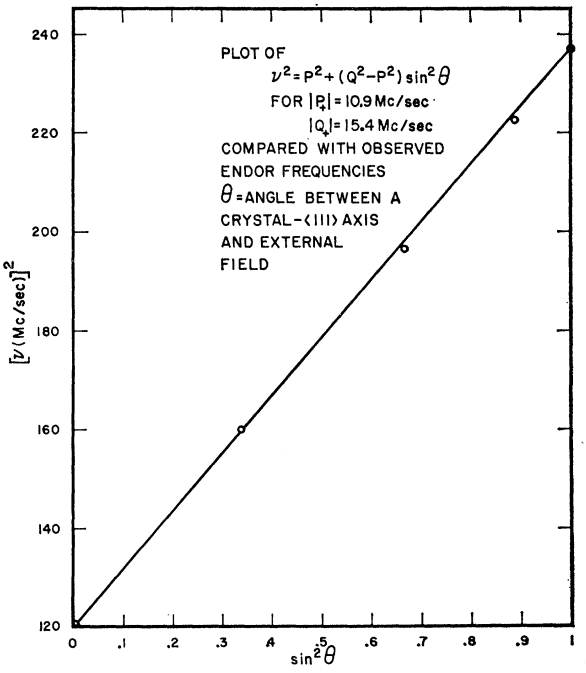

FIG. 10. Fluorine ENDOR frequency as a function of θ, the angle between the external field and a Yb^{3+}-F^- bond. The circles are experimental points.

The crystals, with either a (100) or (110) plane horizontal, were oriented in the cavity by rotating the crystal holder and simultaneously observing the EPR superhyperfine lines on an oscilloscope. In this manner the ⟨100⟩ and ⟨110⟩ directions could be determined since this structure is resolved only along these directions, with best resolution occurring along ⟨100⟩. The crystal was then rotated away from these canonical directions in order to measure the ENDOR frequencies as a function of angle. With the external field along an arbitrary direction in the (100) plane, only two ENDOR lines are expected from the first shell of fluorines for each S_z state. This is because the four fluorines in the (110) plane are equivalent as are the four fluorines in the $(1\bar{1}0)$ plane. Similarly, with the external field in a (110) plane, three ENDOR lines are expected in each S_z state, arising from two pairs and a quartet of equivalent fluorines.

With the external field in the (110) plane, the ENDOR can be measured along each of the axes ⟨001⟩, $\langle 1\bar{1}0\rangle$, and $\langle 1\bar{1}1\rangle$. From the symmetry it is easy to see that for $\langle 1\bar{1}0\rangle$ the quartet of equivalent fluorines has $\theta=\pi/2$, and for $\langle 1\bar{1}1\rangle$ there is a pair for which $\theta=0$. Consequently, from Eq. (22) it is seen that measurements along these axes give directly $|Q|$ and $|P|$, respectively.

The square of the ENDOR frequency is plotted as a function of $\sin^2\theta$ in Fig. 10, where the circles are the experimental points. It is seen that the linear fit to

[22] A. M. Clogston, J. P. Gordon, V. Jaccarino, M. Peter, and L. R. Walker, Phys. Rev. **117**, 1222 (1960).

[23] H. H. Woodbury and G. W. Ludwig, Phys. Rev. **124**, 1083 (1961).

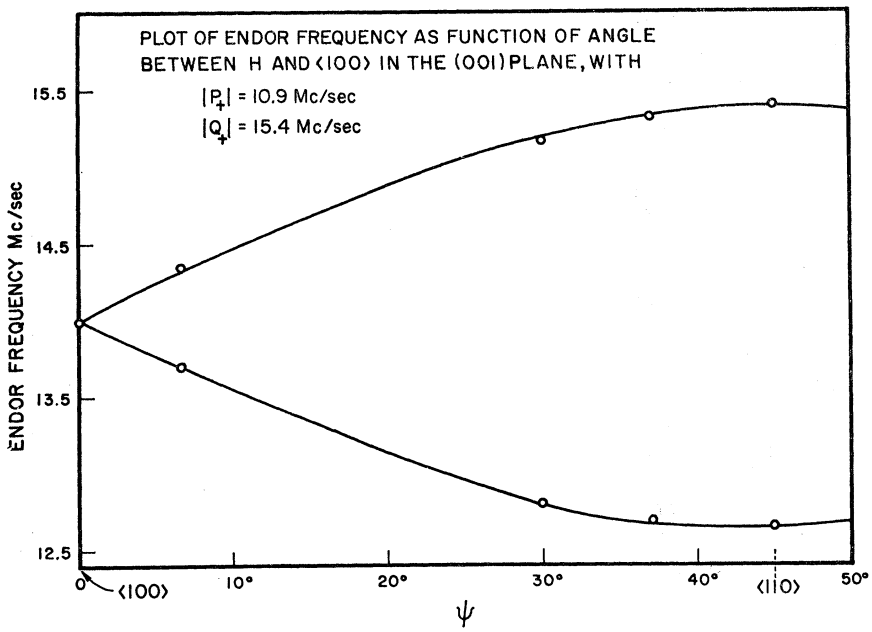

FIG. 11. Angular variation of the ENDOR spectrum in a (001) plane plotted as a function of the angle ψ between the external field and ⟨100⟩. The circles are experimental points.

Eq. (22) is very good. $|P|$ and $|Q|$ are then

$$|P| = 10.90 \pm 0.05 \text{ Mc/sec},$$
$$|Q| = 15.41 \pm 0.05 \text{ Mc/sec}.$$

The calculated and observed angular variations of the ENDOR spectrum in a (100) plane for this particular S_z state are shown in Fig. 11.

Typical ENDOR traces obtained with the field along ⟨110⟩ on several EPR lines are shown in Fig. 12. All lines in this figure are from one S_z state.

As was remarked previously, in order to determine the absolute value of $T_{\parallel}$ and $T_{\perp}$, measurements at different values of H are required. For this purpose ENDOR measurements were performed with H on the two EPR lines of ^{171}Yb (Fig. 12). Results are summarized in Table II. Along ⟨110⟩ one of the two ENDOR lines for each H is equal to $|Q|$, and from Fig. 10 it is seen that $|Q|$ equals the frequency of the higher ENDOR line of each pair. For the central EPR line, $\gamma_N{}^F H = 7.45$ Mc/sec, and

$$|S_z T_{\perp}| > 7.45 \text{ Mc/sec}. \tag{23}$$

By noting the change in $|Q|$ as H is changed, it is found that

$$|S_z T_{\perp} - \gamma_N{}^F H_1| > |S_z T_{\perp} - \gamma_N{}^F H_2|, \tag{24}$$

where $H_1 > H_2$, and therefore $S_z T_{\perp} < 0$.

With (24) we deduce from the other ENDOR line along ⟨110⟩

$$|S_z T_{\parallel} - \gamma_N{}^F H_1| < |S_z T_{\parallel} - \gamma_N{}^F H_2| \tag{25}$$

so that

$$S_z T_{\parallel} > 0. \tag{26}$$

The inequalities (23)–(26) can only hold when

$$\text{Sign} T_{\parallel} \neq \text{Sign} T_{\perp}. \tag{27}$$

No absolute determination of the signs $T_{\parallel}$ and $T_{\perp}$ is possible in this experiment but the ENDOR results for the central EPR line give

$$|T_{\parallel}| = 36.8 \pm 0.1 \text{ Mc/sec},$$
$$|T_{\perp}| = 15.9 \pm 0.05 \text{ Mc/sec}.$$

We now assume that the measured P and Q are P_+ and Q_+ so that the observed ENDOR lines are from the $S_z = +\frac{1}{2}$ state. This implies $T_{\parallel} > 0$ and $T_{\perp} < 0$ and we make this choice in anticipation of the interpretation of $T_{\parallel}$ and $T_{\perp}$ which will be discussed in Part VI. We shall see that this choice is likely to be the correct one and consequently that the ENDOR transition observed are indeed those in the $+\frac{1}{2}$ state.

Once $T_{\parallel}$ and $T_{\perp}$ are determined, the terms P_- and Q_- can be evaluated and the expected ENDOR spectrum in the other S_z state can be calculated.

In Fig. 13 the calculated angular variation of the ENDOR spectrum in a (110) plane for both S_z states

TABLE II. Measured ENDOR frequencies in the $S_z = +\frac{1}{2}$ state on a number of Yb^{3+} EPR lines along ⟨110⟩.

Isotope	$I=0$		$I=\frac{1}{2}$				$I=\frac{5}{2}, I_z=\pm\frac{5}{2}$			
H_0 (gauss)	1860		1540		2108		1465		2234	
ν_n (Mc/sec)	15.41	12.65	14.12	12.94	16.1	12.11	13.63	12.7	16.7	12.47

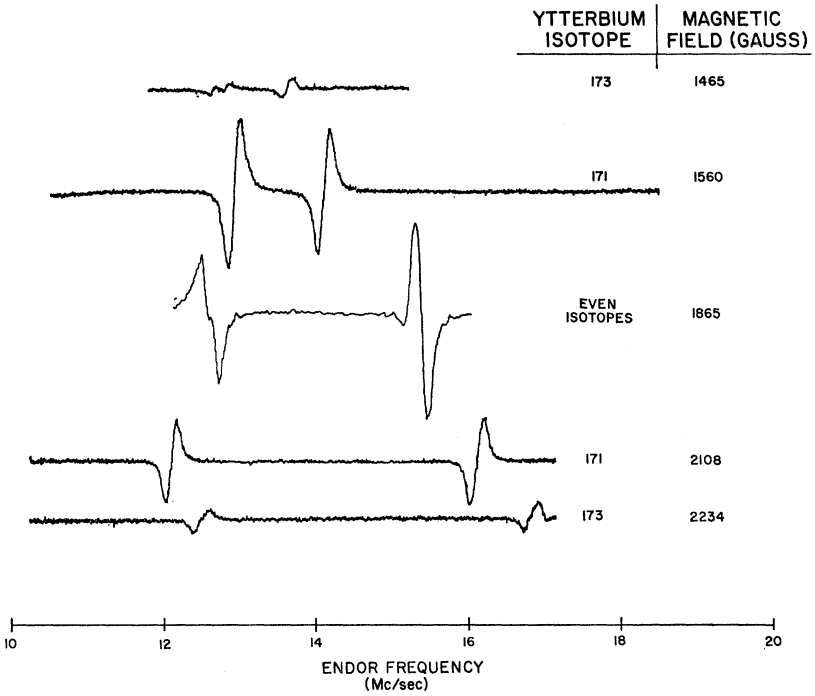

FIG. 12. Typical ENDOR spectra observed with the external field oriented along a ⟨110⟩ direction and sitting on different EPR lines at X band. The traces were obtained at 12–15°K.

is shown. Along ⟨100⟩ the ENDOR lines from the two S_z state should be quite close, but the 14.9-Mc/sec line of the (−) state was never observed in runs at 12–15°K. As indicated by the experimental points in the figure, some lines *were* observed in the (−) state. This was achieved by cooling the sample to the lowest possible temperature with the helium flow system and pushing the sensitivity of the instrument to its upper limit. The power input to the helium bath was six watts and the temperature of the sample below 9°K. It was very surprising to find that these ENDOR lines were more than two orders of magnitude less intense than those from the (+) state. Figure 14 shows the ENDOR lines along ⟨100⟩ with the 6-watt input into the helium bath. Note that the high frequency tail of the (+) line distorts the shape of the (−) line; note also the reduction by a factor of 10^2 in the gain of the instrument as the (+) line is swept. The (−) line in Fig. 14 is about 300 times less intense than the (+) line. This is true also of the other (−) lines observed near ⟨110⟩ and indicated in Fig. 13. We have no explanation for this large difference in intensity of the ENDOR from the two S_z states. In the isoelectronic ion Tm^{2+}, Bessent and Hayes[10] observed the two ENDOR lines along ⟨100⟩ but were unable to see some of the (+) and (−) lines along ⟨110⟩ and ⟨111⟩.

TABLE III. Measured and calculated ENDOR frequencies in Mc/sec in the $S_z=+\frac{1}{2}$ state on the $I=0$ EPR line of Yb^{3+}; $H_0=1860$ G.

Orientation	⟨100⟩	⟨110⟩		⟨111⟩	
Calculated	14.07	12.58	15.41	10.90	14.98
Observed	14.04	12.65	15.41	11.00	14.97

In Table III the calculated and measured ENDOR frequencies for the central EPR line in the (+) state are given for the ⟨100⟩, ⟨110⟩, and ⟨111⟩ orientations.

VI. DISCUSSION

1. Correlation Between the ENDOR and EPR Results

With the superhyperfine tensor parameters T_{II} and $T_{\perp}$ determined from the ENDOR data, the EPR and ENDOR results can be correlated. We begin by considering the central EPR transition at X band, with the external field along a ⟨100⟩ direction.

Figure 15(a) shows the relative intensities of the EPR transitions as a function of magnetic field calculated from Eq. (20). The transition probabilities proportional to $\sin^2(\phi/2)$ are indicated by q while those which vary as $\cos^2(\phi/2)$ are indicated by r. The separation of the superhyperfine levels in the $S_z=+\frac{1}{2}$ and $S_z=-\frac{1}{2}$ states are plotted in Fig. 15(b) as a function of the magnetic field. In this figure,

$$\begin{aligned}\delta(+)&=E^F(+,+)-E^F(+,-),\\ \delta(-)&=E^F(-,+)-E^F(-,-).\end{aligned}\tag{28}$$

The separations were calculated using Eq. (9).

For the central EPR line along ⟨100⟩ we have from Table III and Eqs. (9) and (20)

$$q/r=3,\tag{29}$$

$$\delta(-)-\delta(+)=0.9 \text{ Mc/sec},\tag{30}$$

$$\delta(-)+\delta(+)=29.0 \text{ Mc/sec}.\tag{31}$$

From Fig. 15 it is seen that (30) corresponds to the

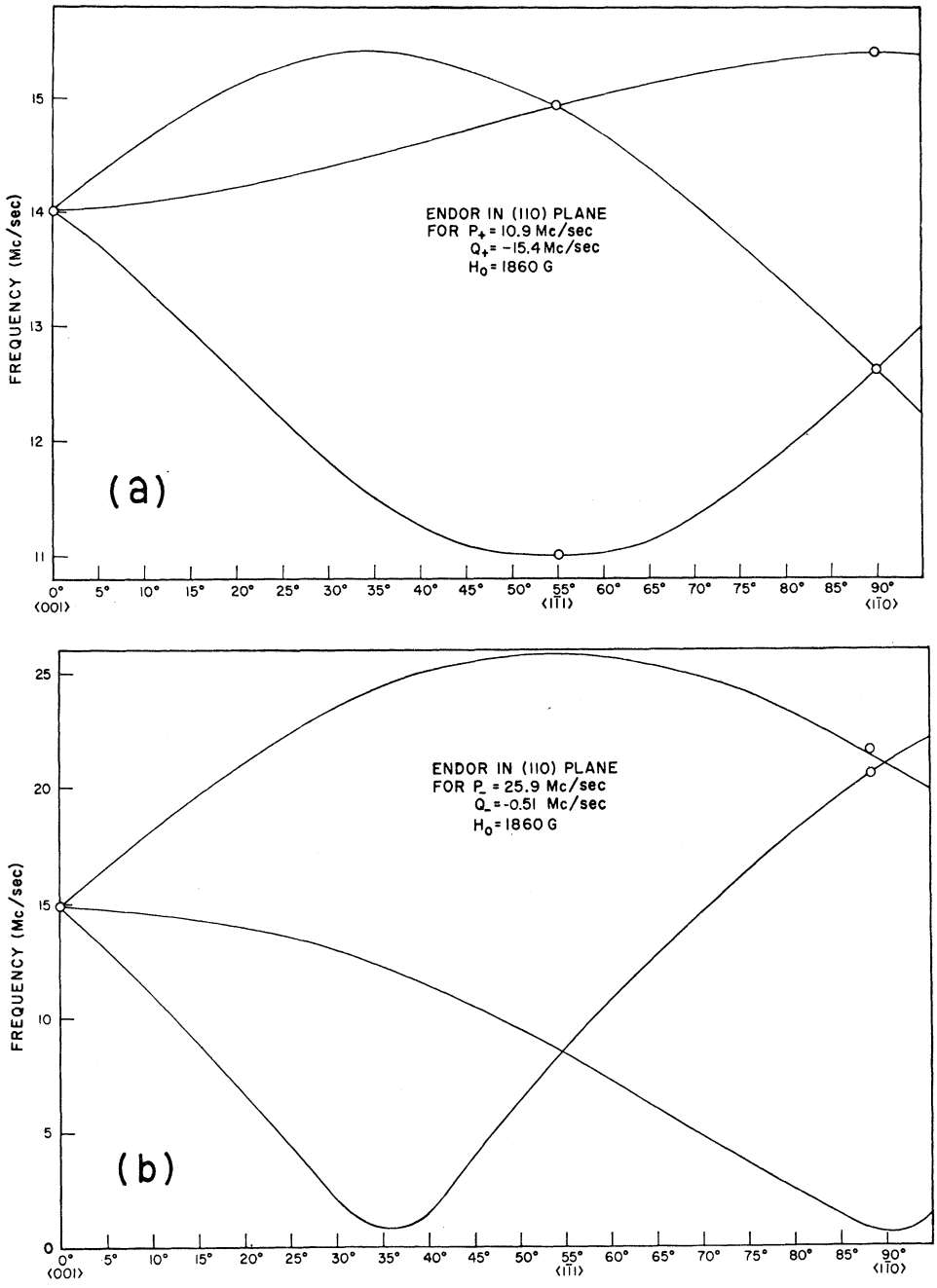

FIG. 13. Calculated angular variation in a (110) plane of the ENDOR spectrum in the two electronic spin states, $S_z=\pm\frac{1}{2}$, where $S=\frac{1}{2}$ is the effective spin of the Γ_7 doublet. Circles are measured ENDOR frequencies.

separation of the two r lines while (31) corresponds to the separation between the q lines. The separation of 0.9 Mc/sec amounts to less than 0.2 G in the EPR splitting, which is less than the observed linewidth. Thus to a good approximation the two r transitions fall on top of each other and therefore the spectrum of the Yb^{3+}-F^- pair should consist of two q lines with a double r line centered halfway between. From (29) and (31) it follows that this triplet should have intensity ratios of 3:2:3 and a separation of 14.5 Mc/sec between adjacent lines. This amounts to 3.01 G, in agreement with the observed splitting of 3.03 G.

One can now construct the total EPR spectrum expected from the 3:2:3 triplets of single fluorine interactions. As far as the EPR is concerned, an "effective" nuclear spin $I'=1$ can be assigned to each fluorine since it gives rise to a three-line structure. Following the standard procedure in hyperfine spectra, one would

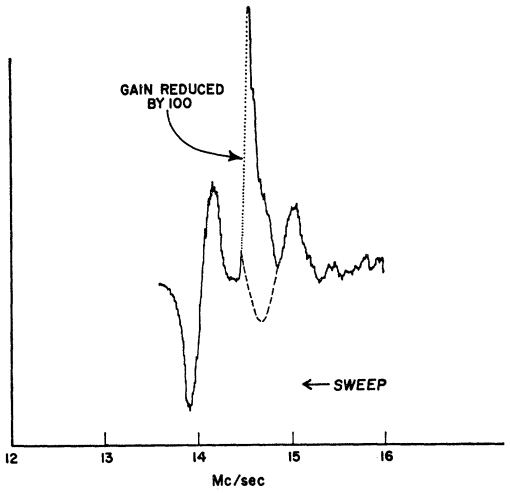

FIG. 14. The ENDOR spectrum at X band with the external field along ⟨100⟩ showing the large difference in intensity of the lines from $S_z=+\frac{1}{2}$ and $S_z=-\frac{1}{2}$ (see text).

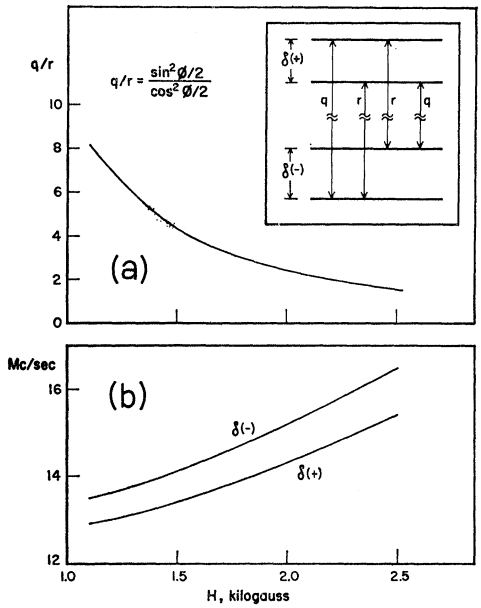

FIG. 15. (a) Relative intensities of the superhyperfine EPR transitions calculated from Equation (20) plotted as a function of the magnetic field with $H\|\langle 100\rangle$, for a Yb^{3+}-F^- pair. The energy-level scheme in the upper right corner indicates the appropriate transitions and separations. (b) Superhyperfine level separations $\delta(+)$ and $\delta(-)$ calculated from Eq. (9).

expect the EPR superhyperfine spectrum along ⟨100⟩ to consist of $\sum_{i=1}^{8} 2I_i'+1=17$ lines. This is in agreement with the number of observed lines.

In Fig. 16 the calculated and observed EPR superhyperfine spectrum of the central Yb^{3+} line along ⟨100⟩, at X band, is shown. The calculated relative intensities are given in Table I. The agreement between the measured and calculated relative intensities is remarkably good.

It is seen from Fig. 15(b) that $\delta(-)-\delta(+)$ is small enough over the whole spread of the X band spectrum so that a 17-line superhyperfine spectrum is expected on each EPR line. Figure 15(a) shows that the ratio q/r decreases from ~10 to less than 2 as the field increases between 1000–2500 G. As q/r decreases, the intensities of the central lines in the superstructure increase, whereas those of the lines out in the wings decrease. Therefore the superhyperfine pattern should become more peaked as the external field increases. This explains the apparent increase in the intensity of

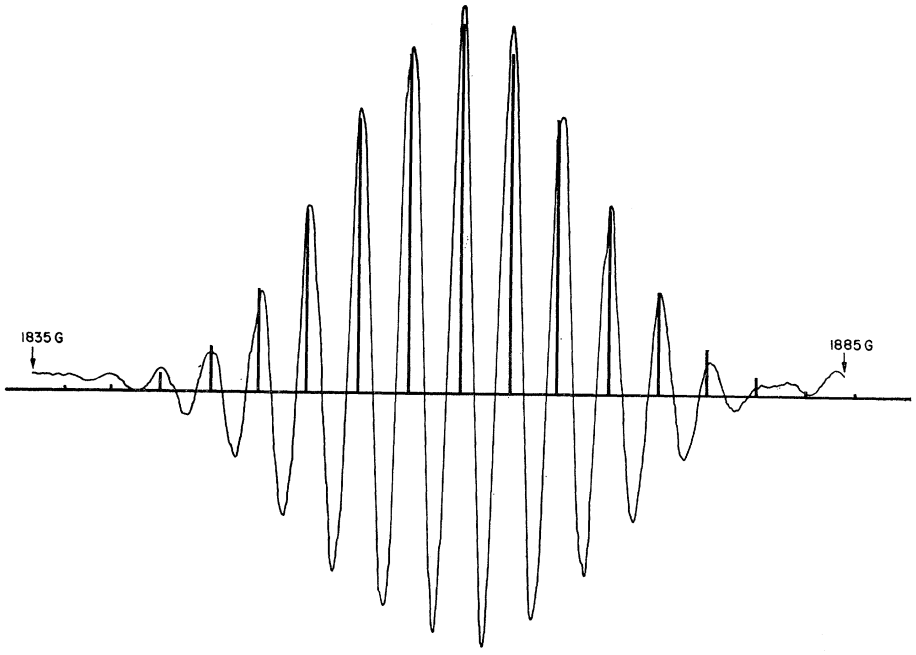

FIG. 16. The observed and calculated superhyperfine structures of the central Yb^{3+} EPR line at X band, along ⟨100⟩.

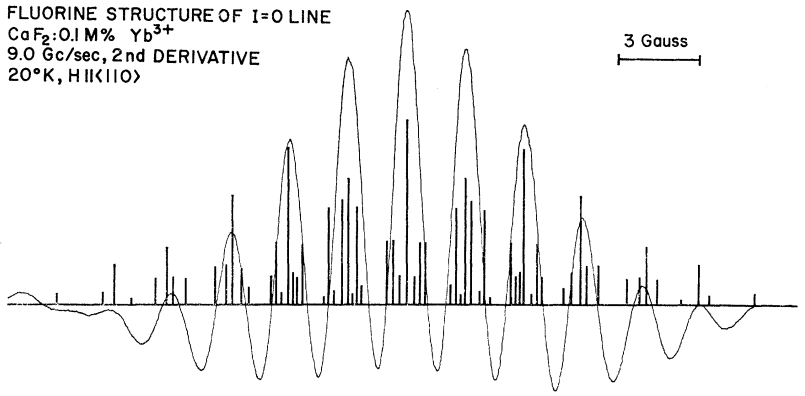

FIG. 17. The observed and calculated superhyperfine structure of the central Yb^{3+} EPR lines at X band, along ⟨110⟩.

the superhyperfine lines with increasing field seen in Fig. 3.

As shown in Table IV, the agreement between the observed and calculated separation of the superhyperfine EPR lines at 35 Gc/sec along ⟨100⟩ is also good (see Fig. 9). From (28), $\delta(-)-\delta(+)=1.5$ Mc/sec at 35 Gc/sec, which is about 0.3 G. In analogy to the X-band case one would expect a 17-line pattern here. However, $q/r\cong 0.2$ and the calculation of the total spectrum shows that the intensity of the lines drops sharply from the center to the wings. The central 9 lines have the following calculated relative intensities:

TABLE IV. The observed and calculated EPR superhyperfine splittings in gauss at X band and 35 Gc/sec for the central line of the ytterbium spectrum.

	X Band		35 Gc/sec	
Orientation	⟨100⟩	⟨110⟩	⟨100⟩	⟨110⟩
Observed	3.03±0.05	3.55±0.05	6.65±0.10	No splitting
Calculated	3.01±0.05	3.46±0.05	6.53±0.05	...

Line	0	±1	±2	±3	±4
Relative intensity	100	60	20	3.5	0.4

The signal-to-noise ratio of the central line in Fig. 9 is about 100 so that it is expected that only the central 7 lines will be observed, in agreement with the experimental results.

We consider now the EPR spectrum at X band along ⟨110⟩. For this orientation there are two groups of four equivalent fluorines. The measured parameters $T_{\parallel}$ and $T_{\perp}$ show that the sums $\delta(-)+\delta(+)$ are 33.6 Mc/sec and 15.9 Mc/sec while for $\delta(-)-\delta(+)$ they are 8.6 Mc/sec and 0.5 Mc/sec. The fact that one sum is almost twice the other and that one difference is close to zero points to a high degeneracy in the fluorine superstructure levels. The total spectrum is composed of a large number of lines which fall into 13 groups, giving rise to the observed 13-line superhyperfine pattern as shown in Fig. 17. The agreement between the calculated and observed spectra seems good. No numbers are given for the relative intensities since the lineshapes of the superhyperfine transitions are not known.

At 35 Gc/sec no simple relations exist between the superhyperfine level separations along ⟨110⟩. Consequently a large number of superhyperfine EPR lines is expected, and it is not surprising that no resolved structure is observed (see Fig. 3).

All observed and calculated superhyperfine splittings are listed in Table IV. It has been shown in this section that the ENDOR measurements account for the unusual features of the EPR spectra in a very satisfactory way.

2. Interaction With More Distant Fluorine Shells

In the present work we have not measured the interaction between the Yb^{3+} ions and more distant fluorine nuclei. Distant fluorines in CaF_2 have been studied by ENDOR in the EPR spectra of divalent europium[9] and divalent thulium.[10] In both cases the interaction is almost pure dipole-dipole. Bessent and Hayes[10] measured the interactions from the second, third, and fourth shell for Tm^{2+} (which is isoelectronic with Yb^{3+}), and found them to be 1.4, 0.6, and 0.35 Mc/sec, respectively. These are the same as predicted by a dipole-dipole calculation.

The largest of these interactions, 1.4 Mc/sec, amounts to a splitting of ~0.3 G. In the case of Yb^{3+} one could expect a slightly stronger interaction since the excess charge on the ytterbium combined with its smaller radius (0.85 Å) may cause some shrinking of the fluorine nearest-neighbor cube. By considering the 24 next-nearest-neighbor fluorines and the probability distribution of their spin alignments, one can account for the observed superhyperfine linewidth of about 2 G.

3. ENDOR Frequency Shifts in ^{171}Yb and ^{173}Yb

So far we have not considered the ENDOR frequencies measured on other than the central EPR lines, except for the determination of the relative signs of $T_{\parallel}$ and $T_{\perp}$.

Typical ENDOR measurements performed along ⟨110⟩ on ^{171}Yb, the two $m=\pm\frac{5}{2}$ lines of ^{173}Yb, and the

TABLE V. Measured and calculated ENDOR frequencies in Mc/sec at X band for a ⟨110⟩ orientation. (Accuracy of calculated frequencies ±0.05 Mc/sec.)

EPR line	Central		Yb(171) $m=+\frac{1}{2}$		Yb(171) $m=-\frac{1}{2}$		Yb(173) $m=-\frac{5}{2}$		Yb(173) $m=+\frac{5}{2}$	
Calculated[a]	15.41	12.58	14.14	12.95	16.39	12.48	13.82	12.98	16.90	12.44
Calculated[b]	···	···	13.97	12.60	16.22	12.13	13.69	12.72	16.77	12.22
Measured	15.41	12.62	14.00	12.85	16.10	12.10	13.63	12.70	16.79	12.47

[a] Calculated from (22).
[b] Calculated from (22) with second order hyperfine correction.

central Yb line are shown in Fig. 12. The measured ENDOR frequencies are listed in the last row of Table V. The appropriate ENDOR frequencies calculated from Eq. (22) are given in the first row of the table. It is seen that the measured frequencies are always lower than those calculated from (22).

It was found that the ENDOR results on other than the central EPR line can be represented by an equation of the form of (28) but the apparent values of $T_{\parallel}$ and $T_{\perp}$ are slightly different for each EPR line. This puzzling feature can be explained when the derivation of Eq. (22) is re-examined.

The Hamiltonian (8) and Eq. (22) were derived by taking $S=S_z$ in the superhyperfine term $\mathbf{S}\cdot\mathbf{T}\cdot\mathbf{I}^F$ for the even Yb isotopes, since in that case the electronic spin is quantized along the external field. But now we are concerned with isotopes which possess a nuclear spin and have a large hyperfine interaction. Taking the ordinary hyperfine spin Hamiltonian with $H\|z$,

$$\mathcal{H}=g\beta HS_z+A(\mathbf{S}\cdot\mathbf{I}), \tag{32}$$

one sees that when A is not very much smaller than $g\beta H$, the electronic (effective) spin will not be oriented along the external field but rather along the resultant of the external and internal fields. This results in a second order shift of the EPR hyperfine spectrum, which is quite pronounced for Yb^{3+} at X band (Fig. 3).

To determine the shift of the ENDOR frequency, we calculate the projection of $\mathbf{S}$ on $\mathbf{H}$ from (32). This "reduced" S_z is used in the Hamiltonian (8) to derive the superhyperfine levels. The Hamiltonian (32) can be written in the form

$$\mathcal{H}=AI_xS_x+AI_yS_y+(g\beta H+AI_z)S_z\equiv g\beta(\mathbf{H}_t\cdot\mathbf{S}), \tag{33}$$

where $\mathbf{H}_t$ is the field acting on the electronic spin

$$|H_t|=(1/g\beta)[(g\beta H+AI_z)^2+A^2(I_x^2+I_y^2)]^{1/2}. \tag{34}$$

Writing $I_z=m$, $I_x^2+I_y^2=I(I+1)-I_z^2$ and taking the scalar product of $\mathbf{H}_t$ with its z component, we get

$$\begin{aligned}S_z&=[1+A^2\{I(I+1)-I_z^2\}/(g\beta H+mA)^2]^{-1/2}S\\&\cong\{1-\tfrac{1}{2}(A/g\beta H_0)^2[I(I+1)-I_z^2]\}S.\end{aligned} \tag{35}$$

In Eq. (8) we replaced $\mathbf{S}$ by S_z since they were identical, but now the projection of $\mathbf{S}$ along z is smaller due to the hyperfine interaction. Thus, all we have to do is to replace S_z in (8) by $S_z(1-x)$ where

$$x=\tfrac{1}{2}(A/g\beta H_0)^2[I(I+1)-I_z^2], \tag{36}$$

and H_0 is the field for the central EPR transition. If we write

$$\begin{aligned}T_{\parallel}'&=(1-x)T_{\parallel},\\T_{\perp}'&=(1-x)T_{\perp},\end{aligned} \tag{37}$$

then all the Eqs. (8)–(23) remain the same with $T_{\parallel}'$ and $T_{\perp}'$ replacing $T_{\parallel}$ and $T_{\perp}$ respectively. It is clear now why the ENDOR results on ^{171}Yb and ^{173}Yb could be represented by Eq. (22) with different values of $T_{\parallel}$ and $T_{\perp}$. Since $x>0$ all the transitions should be shifted to lower frequencies compared with those calculated from (22), in agreement with our observation.

The hyperfine parameters ^{171}A and ^{173}A are known from previous EPR experiments[16] (see Part I) so that the shifts in the ENDOR frequencies due to the hyperfine interactions can be calculated. The second row in Table V shows the ENDOR frequencies calculated with this correction. It is seen that agreement with the measured frequencies is improved substantially.

4. Interpretation of $T_{\parallel}$ and $T_{\perp}$

It was shown in Part IV that the representation of the tensor $\mathbf{T}$ in terms of $T_{\parallel}$ and $T_{\perp}$ is implied by the axial symmetry of the problem. No other assumptions are involved in the derivation of this form of $\mathbf{T}$. Thus expression (4) represents the correct syperhyperfine (or hyperfine) Hamiltonian for all problems involving axial symmetry.

By defining

$$T_s=\tfrac{1}{3}(T_{\parallel}+2T_{\perp}) \tag{38a}$$

and

$$T_p=\tfrac{1}{3}(T_{\parallel}-T_{\perp}), \tag{38b}$$

(4) will have the form

$$\mathcal{H}^F=T_s\mathbf{S}\cdot\mathbf{I}^F+T_p(3S_zI_z^F-\mathbf{S}\cdot\mathbf{I}^F). \tag{39}$$

The first term in the Hamiltonian (39) is an isotropic term while the second has the *form* of a point dipolar interaction. Since (39) is obtained from (4) merely by defining the new constants T_s and T_p, it also is the correct expression for any hyperfine interaction of axial symmetry. It is incorrect, however, to make the physical interpretation that (39) is in fact the sum of an isotropic interaction and a point dipolar interaction. Such an interpretation of (39) amounts to neglecting all

overlap integrals between the paramagnetic ion and its neighboring ions other than the s contact term contained in T_s.

The problem of bonding in rare-earth ions has been considered by Baker and Hurrell[9] and by Bessent and Hayes.[10] In analogy to the extensive treatment of iron group ions,[2,3] molecular orbitals are constructed from the electronic functions of the impurity ion and the ligands. The problem in the rare earths is complicated by the lack of good eigenfunctions for these ions. In addition, not only $4f$ orbitals but also $5s$ and $5p$ orbitals may contribute substantially to the bonding.[1] On the fluorine ligands, $1s$, $2s$, $2p_\sigma$, and $2p_\pi$ orbitals may take part in the bonding. The bonding through the ligand s orbitals is given by T_s while T_p should account for the bonding through the other orbitals, in addition to the dipolar interaction.

In principle, molecular orbitals can be constructed by combining central-ion and ligand-ion single-electron orbitals; Baker and Hurrell[9] and Bessent and Hayes[10] list the various central ion and p ligand orbitals and their representations. It can be inferred that both p_σ and p_π orbitals take part in the bonding in Yb^{3+}. If f_σ and f_π indicate the spin densities in the p_σ and p_π orbitals respectively, the latter authors have shown[10] that the contribution to T_p from the overlap with p orbitals contains terms in f_σ, f_π, and $(f_\sigma f_\pi)^{1/2}$.

In the present case where we have a problem with high symmetry and only the one measurable parameter T_p to account for the p overlap, the spin densities f_σ and f_π cannot in principle be determined.

The empirical values of T_p and T_s can be calculated from Eqs. (38). Our choice of $T_{11}>0$ was made in order to have both T_s and T_p positive. A classical calculation shows that the dipolar interaction between a nearest-neighbor fluorine nucleus and the Yb^{3+} ion in the undistorted CaF_2 lattice contributes 9.81 Mc/sec to T_p. Thus 7.76 Mc/sec is the part of T_p due to charge transfer between the central ion and the p orbitals of its ligands. Had we chosen $T_{11}<0$ we would have $T_p<0$ and $(T_p-9.81)=-27.38$ Mc/sec, which seems to be too large.

As was pointed out previously, the excess charge of Yb^{3+} together with its smaller ionic radius may cause some shrinking of the fluorine cube, resulting in a somewhat larger dipolar interaction. Therefore the value of 7.76 Mc/sec for the anisotropic overlap interaction should be taken with reservation.

The parameters T_s and T_p are given in Table VI where the parameters of the isoelectronic Tm^{2+} are also listed.[10] The table shows that $T_s(Tm^{2+})>T_s(Yb^{3+})$, while $T_p(Tm^{2+})<T_p(Yb^{3+})$. It is reasonable to assume that the electronic cloud of Yb^{3+} will be more localized than that of Tm^{2+} because of the higher positive charge on the Yb nucleus. As a result a smaller contact between the Yb^{3+} electrons and a fluorine nucleus is expected, giving a smaller T_s. On the other hand the extra positive charge of Yb^{3+} will cause the lobes of the fluorine p orbitals to penetrate deeper into the Yb^{3+} electronic cloud resulting in an increased T_p.

TABLE VI. The parameters T_s and T_p for Tm^{2+} and Yb^{3+} in CaF_2. The value of the classical T_p (pure dipole-dipole) is 9.81 Mc/sec.

	T_s (Mc/sec)	T_p (Mc/sec)	References
Tm^{2+}	2.584±0.01	12.283±0.01	10
Yb^{3+}	1.67 ±0.05	17.57 ±0.05	This work

VII. SUMMARY

ENDOR measurements on fluorine nuclei are essential for the understanding of the superhyperfine structure in the EPR spectrum of trivalent ytterbium in CaF_2. The ENDOR results, combined with EPR measurements at 9 Gc/sec and 35 Gc/sec, show that this structure arises from interaction with the nearest neighbor fluorine nuclei which are situated at the corners of the cube surrounding each Yb^{3+} ion. The width of the superhyperfine lines (about 2 G) can be accounted for by dipole-dipole interactions with more distant fluorine nuclei.

The experiments yield the values

$$|T_{11}|=36.8\pm0.1 \text{ Mc/sec}$$

and

$$|T_\perp|=15.9\pm0.05 \text{ Mc/sec}$$

for the diagonal terms of the superhyperfine interaction tensor $\mathbf{T}$. These values account very well for the number, separation, and relative intensities of the EPR superhyperfine lines.

It should be noted that EPR measurements alone can lead to erroneous conclusions since some superhyperfine lines may be unobservable because of low intensity (e.g., at 35 Gc/sec along ⟨100⟩ in the present case, see Fig. 9), or the observed line may be a superposition of many superhyperfine transitions, as in the case here at X band along ⟨110⟩ (see Fig. 17).

An accurate determination of T_{11} and $T_\perp$ is possible only by ENDOR measurements and it was shown that the superhyperfine line intensities are strongly dependent on these parameters.

The large hyperfine splittings in ^{171}Yb and ^{173}Yb give rise to large second order corrections in the EPR spectrum at X band. The influence of these corrections on the ENDOR spectra for these isotopes was detected as a shift in the ENDOR frequencies.

Comparison with ENDOR results on the isoelectronic ion[10] Tm^{2+} show that in Yb^{3+} bonding with the nearest-neighbor fluorines has less s character and more p character than in Tm^{2+}.

ACKNOWLEDGMENTS

It is a pleasure to acknowledge helpful discussions with H. M. McConnell, W. A. Anderson, and H. E. Weaver. We are grateful to K. Lee for the use of his 35-Gc/sec spectrometer and to W. Hayes for a preprint on the ENDOR of CaF_2:Tm^{2+}.